The relative contributions of iron and aluminum oxides to ferrocyanide retention in soils: a comparative study

Y. Wei[1] · R. Yao[1] · S. Chen[1] · H. Zhou[1] · T. Ren[1] · S. Liu[1] · J. Gao[1] · Y. Li[1]

Abstract

Ferrocyanide adsorption onto goethite and gibbsite is normally regarded as an important reaction in cyanide-contaminated soil systems over a broad range of environmental conditions. However, the contribution of these metal oxides to the retention capacity of ferrocyanide by real soil samples remains unclear. This study investigated the adsorption behavior of ferrocyanide onto two representative metal oxides (goethite and gibbsite), as well as its adsorption onto five soil samples containing variable amounts of metal oxides. It was found that the Q_{max} of goethite is much higher than that of gibbsite under comparable pH conditions, indicating the importance of goethite in controlling the geochemical behavior of ferrocyanide in natural soil systems. Ferrocyanide adsorption onto goethite is marginally affected by ionic strength, suggesting its strong affinity to goethite. FTIR results further demonstrated the formation of inner-sphere complexes between goethite and ferrocyanide. No precipitations were detected. Despite the strong affinity of ferrocyanide to these metal oxides, the estimated contribution of goethite to ferrocyanide retention in real soils was quite small, ranging from 1.06 to 8.15%. The results imply that soil components other than these crystalline metal oxides may dominate the retention behavior of ferrocyanide in natural systems.

Introduction

Cyanide plays an important role in many industrial activities, such as electroplating, metal cleaning, and extraction of gold from its ore (Castilla-Acevedo et al. 2020; Moussavi et al. 2018; Zhang et al. 2015; Kuyucak and Akcil 2013; Korte et al. 2000). Cyanide has been frequently detected in soils and aquifers due to spills or leakage during cyanide production and utilization, or to improper disposal of cyanide-containing solid residues (e.g., gas manufacturing by-products and blast furnace sludge) (Wei et al. 2018; Sut-Lohmann et al. 2014; Zhang et al. 2010; Rennert et al. 2007; Rennert and Mansfeldt 2002a; Theis et al. 1994). Anthropogenic cyanide in polluted soils reportedly exists mainly as iron–cyanide complexes (i.e., ferrocyanide $[Fe(CN)_6]^{4-}$ and ferricyanide $[Fe(CN)_6]^{3-}$), with the content of free cyanide (HCN and CN^-) accounting for only a small percentage (Wei et al. 2020; Sut-Lohmann and Raab 2017; Mansfeldt and Höhener 2016; Manar et al. 2011; Johnson et al. 2008). These iron–cyanide complexes, although normally regarded as thermodynamically stable and nontoxic compounds (Shifrin et al. 1996), present a potential health risk due to their tendency to release toxic free cyanide when exposed to sunlight (Rader et al. 1993; Meeussen et al. 1992). In addition to the potential risk posed by dissociation of these iron–cyanide complexes, they also show direct ecotoxicity to some aquatic species, e.g., high chronic toxicity to fleas (Manar et al. 2011). Therefore, more attention should be paid to the geochemical behavior of these metal–cyanide complexes in the soils of cyanide-polluted sites.

In contaminated site soils, the mobility of pollutants is usually controlled by many processes including sorption, complexation, precipitation, and co-precipitation. Of all the processes involved, adsorption normally plays the most significant role, by reducing aqueous concentrations in soil systems. This is particularly true for the ionic pollutants. Gibbsite $(Al(OH)_3)$ and goethite (FeOOH) are

✉ Y. Wei
wym_1982@cqu.edu.cn

1   Key Laboratory of Three Gorges Reservoir Region's Eco-Environment, Ministry of Education, College of Environment and Ecology, Chongqing University, 174 Shazheng Street, Chongqing 400045, People's Republic of China

ubiquitous soil minerals (Cornell and Schwertmann 2003; Violante and Pigna 2002), and these two minerals are normally regarded as the most active soil components controlling the mobility of many cationic (e.g., Pb^{2+}, Cd^{2+}) and anionic pollutants (e.g., PO_4^{3-}, AsO_4^{3-}, CrO_4^{2-}) in soil systems (Arroyave et al. 2018; Xiong et al. 2018; Antelo et al. 2005). Considering their widespread presence and high affinity for many anionic pollutants, sorption of these anions with metal oxides has attracted great attention in the fields of geochemistry and environmental sciences.

The affinity of metal oxides and ionic pollutants is a result of either outer-sphere or inner-sphere complexation. Outer-sphere complexation occurs in such a manner that the ions are physically bound to the mineral surface via electrostatic attractions; ions fixed in this manner are susceptible to environmental conditions and are thus more mobile. Inner-sphere complexation, however, is formed via chemical binding to the mineral surface, becoming part of the surface. In most cases, complete separation between the two mechanisms is difficult, as both outer- and inner-sphere complexation often exist. A study discriminating these two mechanisms is important to understand the mobility and potential risks of many pollutants. From this point of view, it is of great significance to understand the factors (e.g., soil components, pH, ionic strength, etc.) that affect the geochemical behavior of these metal–cyanide complexes.

With regard to the iron–cyanide complexes considered in this study, experiments focusing on individual Al and Fe oxides have been conducted to evaluate their ability to retain these complexes by sorption and/or precipitation (Rennert et al. 2005; Bushey and Dzombak 2004; Rennert and Mansfeldt 2002b, 2001). However, most studies have been concerned only with sorption behavior in the context of one specific soil component, and no systematic comparison has been made among different minerals. Moreover, the contribution of these metal oxides to the fixation of the cyanide complexes in real soil samples has not been systematically studied. Thus, the effect of these metal oxides on Fe–CN retention remains unclear.

The aim of this study was to evaluate the relative importance of iron and aluminum oxides in the retention of iron–cyanide complexes in soils. For this purpose, ferrocyanide sorption behaviors on synthesized metal oxides (goethite and gibbsite), and on five different soil samples, were examined via batch adsorption experiments conducted under various cyanide loading, pH, and ionic strength conditions. During the adsorption experiments, the aqueous cyanide concentration was monitored to evaluate the amount of adsorbed cyanide, and to compare the maximum sorption capacity between the selected metal oxides and soil samples, thus providing an estimation of the relative importance of these metal oxides in ferrocyanide immobilization.

Materials and methods

Preparation of goethite and gibbsite

The goethite used throughout this work was synthesized following a method used by previous researchers (Hiemstra et al. 1989). Briefly, a NaOH solution (5 M) was gradually added (dropwise) to a $Fe(NO_3)_3 \cdot 9H_2O$ solution (0.5 M) under continuous stirring until reaching pH 12. The suspension was stabilized at 60 °C for 90 h and then cooled and centrifuged to remove the liquid phase. The obtained solid phase was subsequently dialyzed with ultrapure water for about 2 weeks until the solution conductivity was < 10 μS/cm. Finally, the suspension was freeze-dried to obtain a goethite powder. Gibbsite was purchased from Sinopharm Chemical Reagent Co., Ltd. The chemicals and reagents utilized in the present study were of AR grade.

Soil sampling and characterization

To investigate the adsorption of ferrocyanide by soils, five soil samples with different physiochemical properties were collected (SPB, JC, FJ, ZY, and BS). The five soils were sampled from four different provinces, namely Chongqing (SPB and FJ), Shanxi (JC), Guizhou (ZY), and Jilin (BS). The SPB, JC, FJ, and ZY soils were sampled from the topsoil (approximately 0–20 cm in depth), and the BS soil, which contained a large amount of soil organic matter (SOM), was purchased from Shenzhibei Agricultural Science and Technology Co., Ltd. All soils were dried at ambient temperature, passed through a 2-mm-mesh sieve, and then gently ground for homogenization.

The properties of the five soils tested are shown in Table 1. The soils were neutral or moderately alkaline except the BS soil, which was acidic. The SOM of the five soils ranged from 0.93 to 22.32%. The cation exchange capacity (CEC) was in the range of 10.10–58.54 cmol/kg. The Al and Fe extracted with acid ammonium oxalate (OX) and dithionite–citrate–bicarbonate (DCB) were quantified by ICP-AES. The oxalate method extracts the amorphous and poorly crystalline fraction of the natural (hydr)oxide fraction (referred to as Fe_{OX} and Al_{OX}) (Roden and Zachara 1996). The DCB method extracts the Fe_{OX}, Al_{OX}, and crystalline Fe and Al oxide phases (referred to as Fe_{DCB} and Al_{DCB}) (Roden and Zachara 1996; Mehra and Jackson 1958). Fe_{DCB}, Fe_{OX}, Al_{DCB}, and Al_{OX} in the five soils were determined to be 8.55–29.03 g/kg, 0.95–15.08 g/kg, 1.12–3.11 g/kg, and 0.29–1.82 g/kg, respectively. The fractions of sand, silt, and clay in the soils, as shown in Table 1, were measured using the

Table 1 Physical and chemical properties of the five soils in this study

Soils	pH 1:2.5 H2O	SOM[a] %	FeDCB[b] g/kg	FeOX[c]	AlDCB[b]	AlOX[c]	CEC[d] cmol/kg	Sand %	Silt	Clay	Texture
SPB	7.55	3.06	11.75	7.06	2.94	0.97	12.80	69.33	10.76	19.90	Sandy clay loam
JC	7.88	1.65	8.55	1.37	1.63	0.29	12.45	42.71	36.83	20.46	Clay loam
FJ	7.71	0.93	12.46	0.95	1.12	0.90	16.40	49.97	27.38	22.65	Clay loam
ZY	6.72	3.21	29.03	6.27	2.27	1.82	10.10	32.58	37.30	30.13	Loamy clay
BS	5.15	22.32	9.94	15.08	3.11	1.18	58.43	43.40	31.85	24.75	Clay loam

[a]*SOM* soil organic matter

[b]Fe_{DCB} and Al_{DCB}: Fe and Al extracted with dithionite–citrate–bicarbonate

[c]Fe_{OX} and Al_{OX},: Fe and Al extracted with acid ammonium oxalate

[d]*CEC* cation exchange capacity, analyzed by the calcium acetate method

hydrometer method (NY/T1121.3-2006) and sorted following the soil textural classification method suggested by the International Society of Soil Science (Kaddah 1974).

Adsorption experiments

Adsorption of ferrocyanide onto the synthesized metal oxides was performed in batch experiments using varying initial concentrations, ionic strengths, and pH. For each experiment, a solution containing the desired concentration of ferrocyanide was prepared at the pre-determined ionic strength and pH. The ferrocyanide solution was then transferred to a brown HDPE bottle containing a goethite (or gibbsite) suspension of the same ionic strength and pH. The volume of the reaction system was set to 25 mL, and the concentrations of goethite and gibbsite were maintained at 5 g/L and 25 g/L, respectively, for all adsorption experiments. The pH after the addition of adsorbent was adjusted using HNO_3 or NaOH solutions. The brown HDPE bottle was placed in a horizontal oscillator at 25 °C and a vibration speed of 180 r/min for 24 h. Then, the solution was filtered through a 0.22 μm membrane filter, and the supernatant was used to determine the cyanide concentration. With this procedure, three sets of adsorption curves were obtained. The first set evaluated the adsorption at electrolyte concentrations of 0.001, 0.01, 0.05, and 0.1 M, with KNO_3 as the electrolyte. The second set was conducted at pH ranging from 3 to 13, and the third set was performed at initial ferrocyanide concentrations of 2×10^{-6} to 4×10^{-3} M. All experiments were repeated twice, and the average values were used.

To evaluate the ferrocyanide sorption capacity of the five soils, batch adsorption experiments were conducted at a solid/liquid ratio of 1:10 (10 g soil to 100 mL water). No pH adjustment or ionic strength control was performed throughout the experiments with the soil reaction systems. The other operational conditions (e.g., temperature, vibration speed, filtration method, etc.) were the same as in previously described experiments with metal oxides.

Analytical methods

The mineralogical characteristics of the two metal oxides (goethite and gibbsite) were determined by X-ray diffraction (XRD) with a PANalytical X'Pert powder diffractometer using Cu Kα radiation at a voltage of 40 kV and current of 40 mA. Minerals were identified using the Inorganic Crystal Structure Database (ICSD). The morphological properties of the two sorbents were investigated by scanning electron microscopy (SEM) with the Zeiss ∑IGMA HD microscope. The FTIR spectra of the samples were determined using the Bruker Vertex 70 spectrophotometer. The specific surface area of the adsorbent was obtained by the BET method using the Quantachrome Quadrasorb 2 MP instrument, and the charging characteristics of the two metal oxides were determined by plotting a zeta potential–pH curve using a zeta potentiometer (Zetasizer Nano ZS90; Malvern). The cyanide concentration in the solution was analyzed following a spectrometric method (HJ484-2009). Briefly, the cyanide-bearing solution was acid-distilled to dissociate the cyanide complexes, and the released free cyanide was absorbed by an alkaline solution. The scrubber solution was then analyzed by a colorimetric method.

Results and discussion

Characterization of goethite and gibbsite

Figure 1a and b presents the morphology of the synthesized goethite sample. Figure 1a shows irregular agglomeration of goethite crystals at a scale of 1 μm. The enlarged SEM image in Fig. 1b shows that the synthesized goethite has a needle-like or rod-like shape, with a crystal size of 200–300 nm, corresponding well with the goethite synthesized in other studies (Xu et al. 2019; Liu et al. 2012). The electron microscope analysis shown in Fig. 1c shows that the purchased gibbsite minerals are randomly distributed,
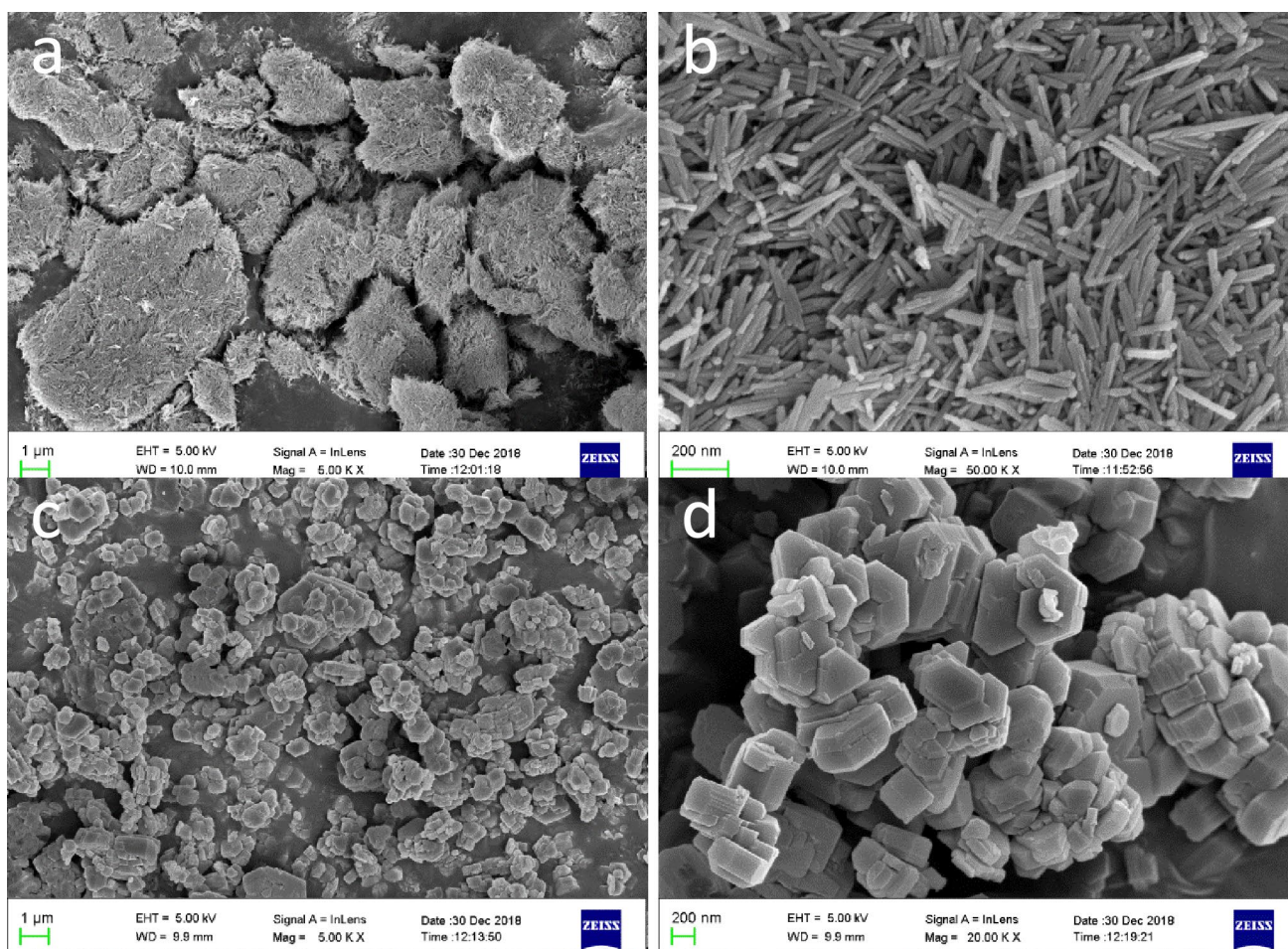
Fig. 1 Electron microscopic images of goethite (**a–b**) and gibbsite (**c–d**)

with a thicker hexagonal plate form about 250–400 nm in diameter, which is typical for the gibbsite, as described by other researchers (Hong et al. 2016; Sweegers et al. 2001).

The XRD patterns of goethite and gibbsite are shown in Fig. S1. The XRD data of goethite indicated a well-crystallized goethite mineral. No diffraction peaks of other oxide or hydroxide minerals were found in this study. The XRD pattern of the purchased gibbsite also indicated that it was a well-crystallized mineral.

Generally speaking, the specific surface area (SSA) of a sorbent is quite important, as a higher SSA normally results in greater adsorption. For goethite, the SSA is known to be related to the drop rate of the alkali solution and the aging time during synthesis (Wu et al. 2012). Within a given time range, a longer aging period normally results in a smaller mineral size and larger SSA of goethite (Liu et al. 2012). When the SSA is less than 60 m²/g, the goethite crystal changes from nano-size to micro-size. The SSA of the synthesized goethite in this study was 92.76 ± 2.19 m²/g, similar to the results reported in other studies using the Hiemstra method (Krumina et al. 2016; Xiong et al. 2015). The SSA

for the commercially purchased gibbsite was 178.92 ± 4.35 m²/g, higher than that of gibbsite samples in previous studies (Xiong et al. 2018; Wu et al. 2000).

The isoelectric point (IEP) values, calculated via linear interpolation using the pH–zeta potential curves (see Fig. S2), were 9.1 and 8.7 for goethite and gibbsite, respectively. The IEP values for goethite and gibbsite in this study were consistent with previously reported values. Previously reported *IEP* values ranged from 6.4 to 9.5 for goethite (Szewczuk-Karpisz et al. 2018a; Madigan et al. 2009; Antelo et al. 2005) and 7.6 to 10.5 for gibbsite (Szewczuk-Karpisz et al. 2018b; Essington and Stewart 2016; Ladeira and Ciminelli 2004).

Effect of ionic strength on ferrocyanide adsorption

The influence of ionic strength on reactions at aqueous interfaces can provide insight into the nature of the chemistry involved. Varying the ionic strength had similar effects on the adsorption of ferrocyanide by goethite and gibbsite (Fig. 2). Generally, ferrocyanide adsorption was
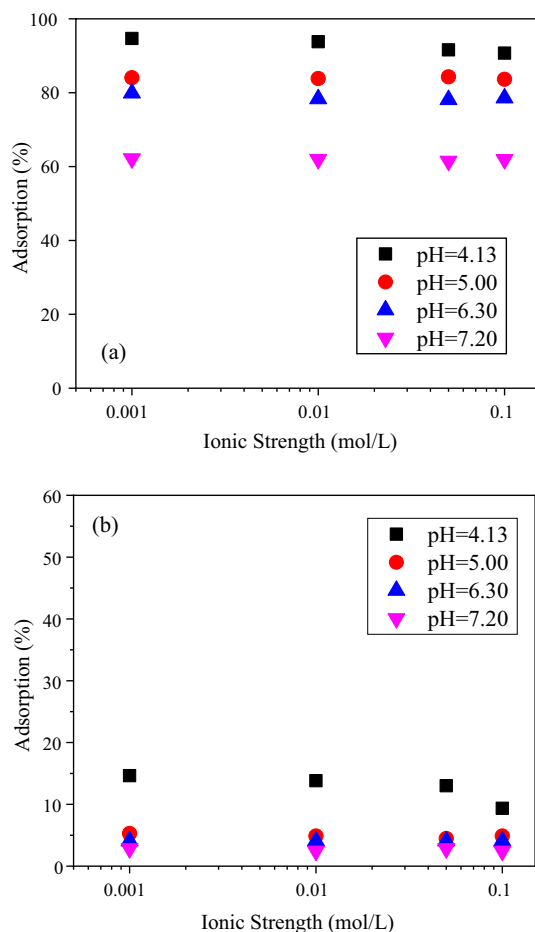
Fig. 2 Effects of ionic strength on adsorption by goethite **a** and gibbsite **b** (0.1 mM ferrocyanide, 5 g/L goethite, and 25 g/L gibbsite)

at pH 5.00, 79–78% and 3.9–3.8% at pH 6.30, and 62–62% and 2.7–2.6% at pH 7.3, respectively.

The effects of the electrolyte concentration on adsorption can be explained in terms of the complexes formed between the adsorbate and the adsorbent. Ions of the supporting electrolyte compete for active sites on the mineral surface with the target adsorbates that adsorb via outer-sphere complexation. Consequently, an elevated electrolyte concentration normally results in a decrease in adsorption. For example, CrO_4^{2-}, SO_4^{2-}, and SeO_4^{2-} are believed to form outer-sphere complexes with $\gamma\text{-}Al_2O_3$, because their adsorption behavior depends strongly on ionic strength (Wu et al. 2000). In contrast, adsorbates that adsorb via inner-sphere complexation are intrinsically chemically bound with the active sites on the mineral surface and are therefore less influenced by changes in the electrolyte concentration. Antelo et al. (2005) evaluated the effects of two different electrolyte concentrations (0.01 and 0.1 M KNO_3) on phosphate and arsenate sorption onto goethite. They observed no obvious salt effect on arsenate adsorption at all pH conditions studied (4.5, 7.0, 9.0, and 10.0). However, the behavior was somewhat different for phosphate: no salt effect was observed under acidic conditions, whereas under neutral and alkaline conditions, an increase in adsorption with increasing electrolyte concentration could be seen. Similar results were found by other researchers (Xu et al. 2019). This is due to the fact that an increased electrolyte concentration decreases electric potential at the particle–liquid interface, consequently reducing the electrostatic repulsion of the ions toward the charged particle surface and thus promoting sorption. However, no such enhancement was observed in the pH ranges studied here, for goethite or gibbsite. The present study found that ionic strength had little influence on ferrocyanide sorption. This result at least showed that inner-sphere complexation played a dominant role when ferrocyanide adsorbed onto goethite or gibbsite.

Effect of pH on ferrocyanide adsorption

Figure 3a and b presents data for the pH-dependent fraction of sorbed ferrocyanide (%), with initial ferrocyanide concentrations ranging from 0.01 to 0.15 mM for the goethite system and from 0.005 to 0.1 mM for the gibbsite system. For the two metal oxides, ferrocyanide adsorption declined with increasing pH, which was identical to the general pH-dependent sorption behavior of anions (e.g., PO_4^{3-}, AsO_4^{3-}, etc.) when performing adsorption onto oxide minerals (Xu et al. 2019; Arroyave et al. 2018; Wu et al. 2000). The goethite and gibbsite systems differed, as ferrocyanide adsorption on goethite was higher across the pH range and was still significant at pH over the IEP. When the ferrocyanide concentration was 0.01 mM, the sorbed fraction by goethite remained above 99% until the pH reached 10.5. Above pH
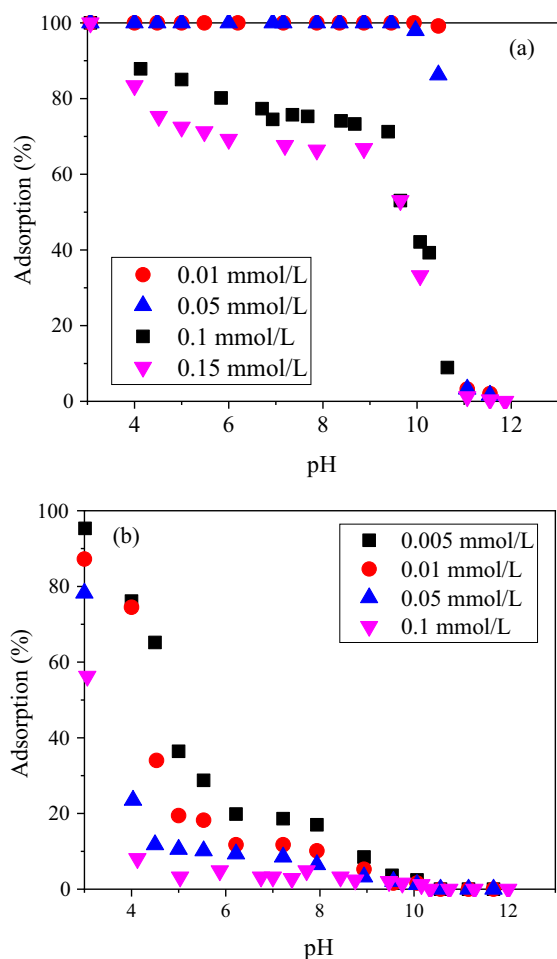
marginally affected by ionic strength, except at pH 4.13. At this low pH level, the adsorption ratio decreased from 95 to 90% for goethite and from 15 to 9.5% for gibbsite with increasing electrolyte concentrations from 0.001 to 0.1 M. This phenomenon may be partially explained as follows. First, at pH 4.13, a significant proportion of ferrocyanide presents as $[HFe(CN)_6]^{3-}$, which is expected to have a lower affinity to the positively charged goethite surface; second, under such an acidic condition, a proportion of ferrocyanide is assumed to have been transformed to ferricyanide. Previous researchers reported that ferrocyanide and ferricyanide could easily be inter-transformed under appropriate conditions (Huang et al. 2007). The formation of ferricyanide was supported by the appearance of a light yellow color in the adsorption system at pH 4.13. Additional research conducted by our group found that ferricyanide was more susceptible to ionic strength than ferrocyanide. Under other pH scenarios, with increased ionic strength, the ferrocyanide adsorption fraction on goethite and gibbsite varied in the ranges of 84–83% and 5.5–5.2%

Fig. 4 FTIR spectra of ferrocyanide adsorbed on goethite at different pH values

Fig. 3 pH-dependent ferrocyanide sorption onto goethite **a** and gibbsite **b** in 0.05 M NaNO$_3$. Different symbols represent different ferrocyanide concentrations: 0.01–0.15 mM for the goethite system and 0.005–0.1 mM for the gibbsite system

10.5, the adsorption ratio declined rapidly, dropping to 3.5% at pH 11. When ferrocyanide was 0.05 mM, the adsorption ratio was 87% at pH 10.5 and quickly dropped to 3% at pH 11; at 0.1 mM, the adsorption ratio was 72% at pH 9.5 and then dramatically decreased to 1% at pH 11; and when ferrocyanide was 0.15 mM, a similar but slightly lower sorption ratio was observed compared to that at 0.1 mM. From these results, we concluded that at lower adsorbate concentrations, the position of the adsorption edge at a given solid concentration is independent of the adsorbate concentration, as observed in the present study for ferrocyanide concentrations up to 0.05 mM. At higher adsorbate concentrations, the pH edge was shifted to lower pH points, which may result, for example, from saturation effects of surface binding sites (e.g., ≡FeOH for goethite). For gibbsite, a quite different sorption trend and much lower sorption ratio were observed. When the pH approached its IEP (8.7 for gibbsite), the sorption ratios were below 10% under all four scenarios.
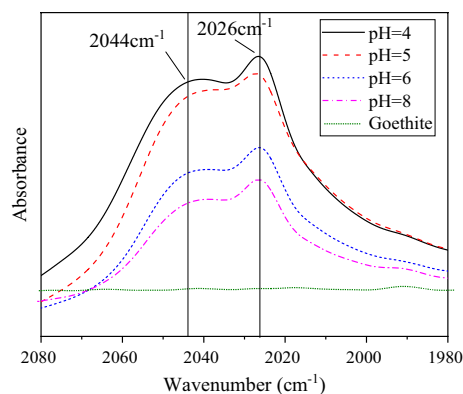
The affinity between adsorbent and adsorbate is highly dependent on the characteristics of the adsorbent (e.g., SSA and charging characteristics), as well as on the chemical speciation of the adsorbate. The pH-dependent ferrocyanide sorption onto goethite and gibbsite may have been caused by pH-dependent variation in adsorbent and adsorbate characteristics. All pKa values for ferrocyanic acid were reportedly lower than 4.5 (e.g., pK$_3$ = 2.2 and pK$_4$ = 4.2), implying that the pH had little influence on the speciation of ferrocyanide in most experiments in this study. In other words, most ferrocyanide ions present as [Fe(CN)$_6$]$^{4-}$, except under experimental scenarios with pH below 4.5. The significant influence of pH on ferrocyanide sorption was thus mainly ascribed to the charging characteristics of the sorbent. For amphoteric minerals such as goethite and gibbsite, higher pH leads to a more negatively charged mineral surface, resulting in stronger repulsion between the adsorbent and anionic adsorbate, whereas a lower pH results in more positive charge on the mineral surface, thus making the adsorbent more attractive to the anions. A striking finding was that the ferrocyanide sorption was still observed at pH values higher than the IEP of goethite, which further indicated that mechanisms other than electrostatic interactions, such as specific adsorption, were involved.

FTIR analysis

The FTIR spectra of goethite before and after sorption are shown in Fig. 4. The FTIR analysis of the gibbsite system provided no valuable information due to the low sorption capacity of gibbsite even at low pH; therefore, the data are not shown here. The FTIR spectrum of goethite before sorption further indicated a pure mineral without contamination. The spectra of the goethite minerals after ferrocyanide sorption were not a simple overlaying of the spectra of goethite (before sorption) and [Fe(CN)$_6$]$^{4-}$, as the characteristic spectrum of [Fe(CN)$_6$]$^{4-}$ at 2044 cm^{-1}

split into two peaks (at 2044 and 2026 cm^{-1}) after sorption. This is an indication that ferrocyanide was not solely adsorbed as outer-sphere complexes, since a new bond was detected spectroscopically. Two bands, at 2026 cm^{-1} and 2043 cm^{-1}, were found for the four samples adsorbed at different pH conditions. These bands, although varying in strength, did not change position or shape. The increasing band strength with decreased pH should be related to the increased sorption amount of ferrocyanide. Therefore, the band at 2026 cm^{-1} can be ascribed to the chemical binding of ferrocyanide to the goethite surface, e.g., formation of a monodentate or bidentate inner-sphere complex, while the spectrum at 2044 cm^{-1} represents sorbed ferrocyanide via an electrostatic attraction with the goethite surface.

The interaction of ferrocyanide and metal oxides may include two-dimensional adsorption (accumulation of ferrocyanide at the oxide–solution interface) and three-dimensional precipitations (formation of an insoluble product). However, no precipitation of cyanide-containing products (e.g., Berlin blue, with a characteristic band at 2092 cm^{-1}) as a result of the reaction of ferrocyanide with metal oxides was found in the present study.

Sorption capacities of ferrocyanide: metal oxides versus soil samples

The results presented above provide some essential information for understanding the mechanisms involved when ferrocyanide reacts with goethite and gibbsite. However, the relative importance of these metal oxides in terms of the retention of ferrocyanide in real soil samples remains unclear. Therefore, we performed additional isothermal adsorption experiments with varying cyanide concentrations and then fitted a Langmuir model to obtain the maximum sorption capacities of both synthesized oxides and soil samples. By combining the content of Fe_{DCB}, Fe_{OX}, Al_{DCB}, and Al_{OX} in the soils used in this study, we can roughly estimate the contribution of these metal oxides to the immobilization of ferrocyanide in natural soils.

Figure 5a and c shows the sorption isotherms of ferrocyanide on goethite and gibbsite. The sorbed fraction of ferrocyanide on these two minerals is also plotted in Fig. 5b and d for better differentiation of their sorption behavior at different pH values. The adsorption results were fitted to the Langmuir model and Freundlich model (Eqs. (1 and 2)), and the results are summarized in Table 2.

Fig. 5 Adsorption isotherms of ferrocyanide onto goethite (**a–b**) and gibbsite (**c–d**) in 0.01 M NaNO$_3$
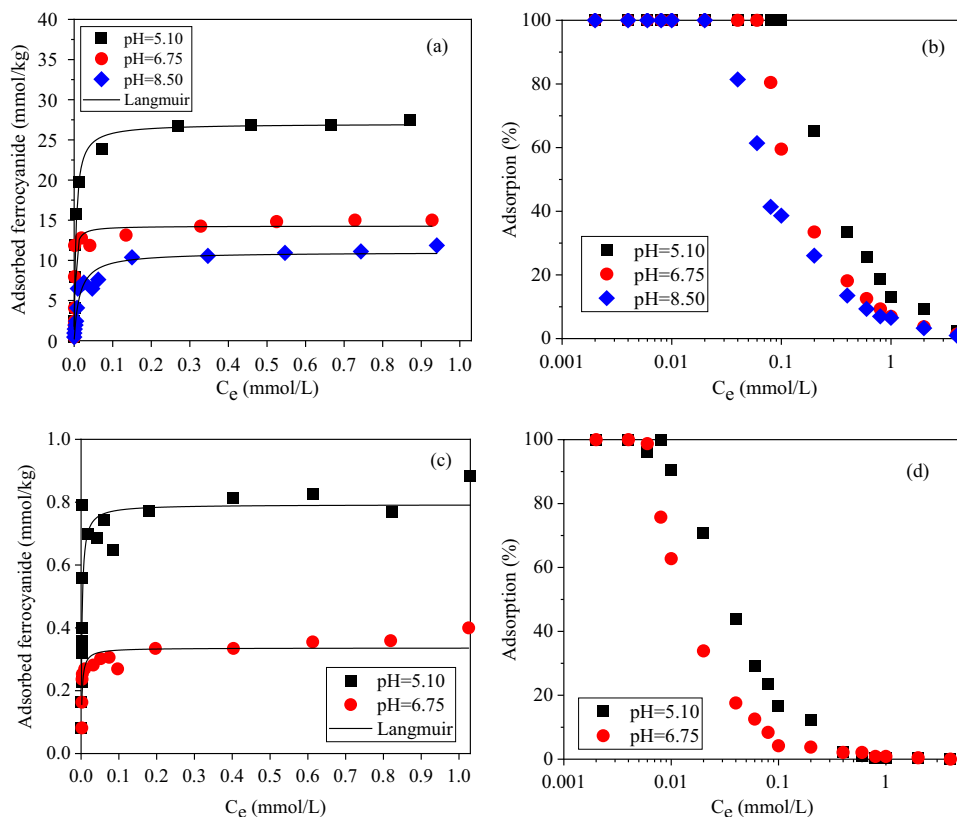
Table 2 Langmuir and Freundlich fitting parameters of ferrocyanide adsorption onto pure metal oxides and soil samples

	Q_{max} (mmol/kg)	K_L (L/mmol)	R^2	K_F (mmol$^{1-(1/n)}$L$^{1/n}$/kg)	n	R^2
Goethite						
pH = 5.10	28.90	314.07	0.8077	29.77	19.20	0.8065
pH = 6.75	14.53	164.85	0.7873	14.88	14.07	0.7944
pH = 8.50	10.93	28.10	0.9398	11.97	6.26	0.8660
Gibbsite						
pH = 5.10	0.77	465.92	0.9132	0.91	8.98	0.7395
pH = 6.75	0.31	434.55	0.6829	0.39	7.51	0.6319
Soil samples						
SPB	22.06	1.36	0.9863	5.79	2.52	0.9180
JC	10.90	0.22	0.9947	2.94	2.62	0.9186
FJ	13.58	0.35	0.9903	5.08	3.39	0.8927
ZY	15.71	0.22	0.9887	4.16	2.58	0.9545
BS	41.73	2.30	0.9862	12.77	2.79	0.8805

$$q_e = \frac{Q_{max}K_L C_e}{\left(1 + K_L C_e\right)}, \tag{1}$$

$$q_e = K_F C_e^{\frac{1}{n}} \tag{2}$$

where q_e is the amount of sorbed ferrocyanide (mmol/kg); Ce is the concentration of ferrocyanide in the liquid phase after equilibrium (mmol/L); Q_{max} and K_L are Langmuir parameters related to the monolayer sorption capacity (mmol/kg) and sorption affinity coefficient (L/mmol), respectively (Wei et al. 2014; Yan et al. 2010; Wisawapipat al. 2009); n (dimensionless) and K_F (mol$^{1-(1/n)}$L$^{1/n}$/kg) are empirical Freundlich parameters representing the sorption intensity and capacity, respectively (Wei et al. 2014).

The purpose of this set of experiments was to determine the maximum sorption amount of ferrocyanide on these two minerals. The Q_{max} values calculated from the Langmuir model revealed a great disparity between goethite and gibbsite under comparable pH conditions, e.g., the Q_{max} for goethite at pH 5.1 was 28.9 mmol/kg, which is 35 times higher than that for gibbsite. These results seem incompatible with the SSA of these two minerals, which are 92 m^2/g for goethite and 178 m^2/g for gibbsite. A study conducted by Bushey and Dzombak (2004) also noted the low sorptive capacity of ferrocyanide on gibbsite. However, it should be noted that the gibbsite used in that study had a low SSA (0.1 m^2/g), which is quite different from the gibbsite used here. The Freundlich adsorption capacity parameters (K_F) of the goethite sample were all higher than those of gibbsite at comparable pH conditions, which is indicative of the stronger affinity of goethite for ferrocyanide adsorption. Considering the results above, we concluded that the contribution of gibbsite to ferrocyanide retention is negligible in soil systems despite its surface characteristics. Therefore, only goethite was considered when evaluating the contribution of these metal oxides to the retention of ferrocyanide by soils.

The five soils used in this study were characterized by different physiochemical properties (Table 1). The isothermal adsorption curves of ferrocyanide by the five soils are presented in Fig. 6. The Langmuir and Freundlich fitting parameters are listed in Table 2. The adsorption data revealed that the five soils showed quite different sorption capacities of ferrocyanide, ranging from 11.90 to 41.73 mmol/kg. However, no correlation was found between the sorption capacity and total content of active iron oxides (Fe$_{DCB}$). To evaluate the contribution of goethite to the retention of ferrocyanide in real soils, we assumed that all active iron oxides present were goethite. Based on this assumption, the contribution of goethite (R%) was roughly estimated using Eq. (3).
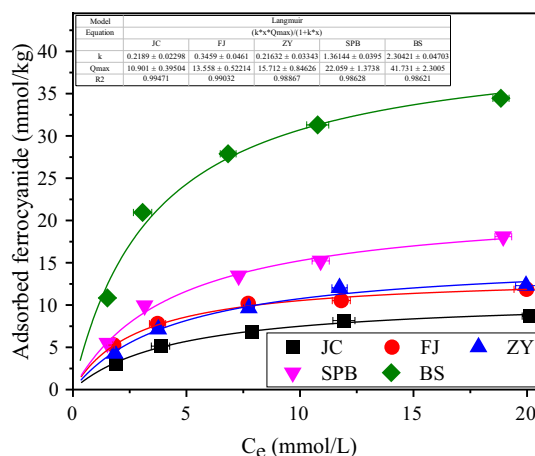
Fig. 6 Adsorption isotherms of ferrocyanide onto different soil samples

$$R\% = \frac{89 \times Q_{\mathrm{max}-G} Fe_{\mathrm{DCB}}}{10 \times 56 \times Q_{\mathrm{max}-S}}\%, \qquad (3)$$

where $Q_{\mathrm{max}-G}$ and $Q_{\mathrm{max}-S}$ are the adsorption capacities of goethite and soil samples derived from the Langmuir fitting results (mmol/kg), respectively; Fe_{DCB} is the amount of total active iron oxides in soils; and 89 and 56 in the equation are the molecular weights of Fe and FeOOH, respectively.

The calculated results are shown in Table 3. It is obvious that the contribution of goethite was no more than 9% for all soils investigated, revealing the low significance of goethite with respect to the retention of ferrocyanide in natural soils. These results suggest the presence of other mechanisms controlling the mobility of Fe–CN in soils (e.g., precipitation). The sorption capacity was highest for BS soil, which had the lowest pH, and lowest for the JC soil, which had the highest pH. This was consistent with trends for the active metal oxides in soils (e.g., goethite and gibbsite) on the sorption of ferrocyanide, whereby a decreased pH normally leads to increased sorption of ferrocyanide. Furthermore, acidic soil may favor the precipitation of cyanide-bearing compounds (e.g., Berlin blue) (Sut-Lohmann et al. 2015), which further promotes the partitioning of cyanide into the soil solid phase. Additionally, the high content of SOM in the BS may also be a non-negligible factor affecting its sorption behavior. However, further research is required to verify this hypothesis.

We demonstrated the strong affinity of goethite for ferrocyanide in Sect. "Effect of ionic strength on ferrocyanide adsorption"; however, the sorption capacity of goethite with ferrocyanide was quite low when compared to other equivalent anions (e.g., PO_4^{3-}), which led directly to the low $R\%$ values (Table 3). Phosphate is an anion commonly found in soils. Moreover, the association of phosphate with many metal oxides (e.g., goethite, gibbsite, ferrihydrite, etc.) has been extensively studied (Tiberg et al. 2020; Arroyave et al. 2018; Wei et al. 2014). Comparison of the sorptive behavior

Table 3 Estimated contribution of goethite to the retention of ferrocyanide in soils

	JC	FJ	ZY	SPB	BS
$Q_{\mathrm{max}-S}$ (mmol/kg)[a]	10.90	13.56	15.71	22.06	41.73
Fe_{DCB} (g/kg)[b]	8.55	12.46	29.03	11.75	9.94
$Q_{\mathrm{max}-G}$ of goethite (mmol/kg)[c]	27.88	27.88	27.88	27.88	27.88
$R\%$[d]	3.48	4.07	8.19	2.36	1.06

[a]Data obtained from the Langmuir fitting results of different soil sorption systems

[b]content of active iron oxides in the soils

[c]data obtained from the Langmuir fitting results of the goethite sorption systems (Q_{max} obtained at pH = 5.10 was used in the calculation)

[d]contribution of goethite to retention of ferrocyanide ($R\%$) calculated as $R\% = [89 \times Q_{\mathrm{max}-G} \times Fe_{\mathrm{DCB}}/(10 \times 56 \times Q_{\mathrm{max}-S})]\%$

of phosphate and ferrocyanide should provide more insight into the interaction mechanisms of ferrocyanide with metal oxides. Table 4 summarizes the reported Q_{max} for phosphate on goethite and gibbsite samples. The Q_{max} of phosphate on goethite ranged from 70 to 336 mmol/kg with a pH of 4–10 and electrolyte concentration of 0.01 M KCl/KNO$_3$, which is dozens of times higher than that for ferrocyanide. Moreover, gibbsite has also been shown to be an effective sorbent for phosphate, with Q_{max} ranging from 225 to 389 mmol/kg, which is approximately 100 times that of ferrocyanide. We cannot yet provide a definitive explanation of this discrepancy. When we make such comparisons, we should always keep in mind that the Q_{max} value stands for an apparent sorption maximum under specific conditions (e.g., ionic strength and pH) and is not necessarily identical to the total number of active groups on the mineral surface. One plausible explanation for the dissimilar sorptive behaviors of phosphate and ferrocyanide might be the steric match (or geometric match) between the active site and sorbed species.

Tiberg et al. (2020) evaluated the sorption behavior of arsenate and phosphate on poorly crystalline iron (Fh) and aluminum hydroxide (Alhox), and found a higher affinity of phosphate on Alhox and a higher affinity of arsenate on Fh. They ascribed the specific affinities of arsenate/Fh and phosphate/Alhox to the steric match. Arsenate and phosphate are believed to exist mainly as bidentate complexes on Alhox and Fh via ligand exchange for –OH$_2$ and –OH on mineral surfaces. The distance between two oxygen atoms in the phosphate and arsenate tetrahedra was compared with the distance between two neighboring oxygen atoms on the mineral surfaces. The authors found that the edge length of an Fe octahedron (in Fh) was approximately 2.6–3.0 Å, fitting better with the arsenate tetrahedron (~ 2.7 Å), whereas the Al octahedron, with a smaller edge length (approximately 2.5–2.9 Å), fit better with the phosphate octahedron (~ 2.5 Å). Ferrocyanide has an octahedron geometry, and the distance between two adjacent N atoms in the octahedron was calculated to be 4.55 Å based on its geometry (Prampolini et al. 2014), which is much larger than that of phosphate (~ 2.5 Å). This may be the major factor inhibiting its combination with goethite and gibbsite.

Conclusion

To evaluate ferrocyanide migration in natural systems, the sorption performance and nature of sorption onto goethite and gibbsite at different pH levels and electrolyte concentrations were evaluated. Changes in the ionic strength had no obvious effect on ferrocyanide sorption by goethite and gibbsite. Ferrocyanide adsorption onto the two minerals declined with increasing pH values, which was consistent with the sorption patterns of other high-valence anions (e.g.,

Table 4 Comparison of the sorptive capacities of ferrocyanide and phosphate on goethite and gibbsite

References	This study	Wei et al. 2014	Antelo et al. 2005	Violante and Pigna 2002
Adsorbent	Goethite	Goethite	Goethite	Goethite
SSA(m^2/g)	92	51	70.8	85
IEP	9.1	8.2[a]	9.3	7.8[b]
Sorbate	$Fe(CN)_6^{4-}$	PO_4^{3-}	PO_4^{3-}	PO_4^{3-}
Adsorbent dose (g/L)	5	1	14	1~6
Electrolyte concentration (mol/L)	0.01 $NaNO_3$	0.01 KCl	0.01 KNO_3	0.05 KCl
Qmax (mmol/kg)	28.9 (pH 5.1)	336 (pH 5.0)	160 (pH 4.5)	160 (pH 4)
	14.5 (pH 6.7)	–	120 (pH 7.0)	158 (pH 5)
	10.9 (pH 8.5)	–	100 (pH 8.5)	136 (pH 7)
	–	–	70 (pH 10)	–

References	This study	Hong et al. 2016	Violante and Pigna 2002
Adsorbent	Gibbsite	Gibbsite	Gibbsite
SSA (m^2/g)	178	–	120
IEP	8.7	–	8.9[b]
Sorbate	$Fe(CN)_6^{4-}$	PO_4^{3-}	PO_4^{3-}
Adsorbent dose (g/L)	25	–	1–6
Ionic strength (mol/L)	0.01 $NaNO_3$	0.001 NaCl	0.05 KCl
Qmax (mmol/kg)	0.77 (pH 5.1)	389 (pH 5.0)	318 (pH 4)
	0.31 (pH 6.7)	–	280 (pH 5)
	–	–	225 (pH 7)

[a]Point of zero charge (PZC)

[b]Point of zero salt effect (PZSE)

PO_4^{3-}, AsO_4^{3-}, etc.). For ferrocyanide, the sorption capacity of goethite was much greater than that of gibbsite. One possible explanation for this is that the geometric size of ferrocyanide is better matched to that of goethite than gibbsite. An FTIR spectrum analysis proved the existence of chemical bonding of ferrocyanide with the goethite surface. However, the nature of sorbed ferrocyanide species on goethite and gibbsite over a broad range of environmental conditions still needs further exploration. Despite the strong affinity of ferrocyanide for goethite, the sorption capacity Q_{max} is low compared to that of other anions. Based on a rough estimation using laboratory experiment-derived parameters (including Q_{max} and Fe_{DCB}), we consequently concluded that the contribution of these metals oxides to the retention of ferrocyanide in natural soils is relatively small.

Declarations

Conflict of interest The authors declare that they have no conflict of interest.

References

Antelo J, Avena M, Fiol S, Lopez R, Arce F (2005) Effects of pH and ionic strength on the adsorption of phosphate and arsenate at the goethite–water interface. J Colloid Interf Sci 285(2):476–486. https://doi.org/10.1016/j.jcis.2004.12.032

Arroyave JM, Puccia V, Zanini GP, Avena MJ (2018) Surface speciation of phosphate on goethite as seen by InfraRed surface titrations (IRST). Spectrochim Acta A 199:57–64. https://doi.org/10.1016/j.saa.2018.03.043

Bushey JT, Dzombak DA (2004) Ferrocyanide adsorption on aluminum oxides. J Colloid Interf Sci 272(1):46–51. https://doi.org/10.1016/j.jcis.2003.09.024

Castilla-Acevedo SF, Betancourt-Buitrago LA, Dionysiou DD, Machuca–Martinez F (2020) Ultraviolet light–mediated activation of persulfate for the degradation of cobalt cyanocomplexes.

J Hazard Mater 392:122389. https://doi.org/10.1016/j.jhazmat.2020.122389

Cornell RM, Schwertmann U (2003) The iron oxides: structure, properties, reactions, occurrences and uses. Wiley–VCH, Weinheim

Essington ME, Stewart MA (2016) Adsorption of antimonate by gibbsite: reversibility and the competitive effects of phosphate and sulfate. Soil Sci Soc Am J 80:1197–1207. https://doi.org/10.2136/sssaj2016.04.0129

Hiemstra T, Van Riemsdijk WH, Bolt GH (1989) Multisite proton adsorption modeling at the solid/solution interface of (hydr) oxides: a new approach: application to various important (hydr) oxides. J Colloid Interf Sci 133(1):91–104. https://doi.org/10.1016/0021-9797(89)90284-1

Hong ZN, Li JY, Jiang J, Li ZL, Xu RK (2016) Competition between bacteria and phosphate for adsorption sites on gibbsite: An in-situ ATR–FTIR spectroscopic and macroscopic study. Colloid Surface B 148:496–502. https://doi.org/10.1016/j.colsurfb.2016.09.026

Huang TH, Salter G, Kahn SL, Gindt YM (2007) Redox titration of ferricyanide to ferrocyanide with ascorbic acid: illustrating the Nernst equation and Beer–Lambert law. J Chem Educ 84(9):1461–1463. https://doi.org/10.1021/ed084p1461

Johnson CA, Grimes DJ, Leinz RW, Rye RO (2008) Cyanide speciation at four gold leach operations undergoing remediation. Environ Sci Technol 42(4):1038–1044. https://doi.org/10.1021/es702334n

Kaddah MT (1974) The hydrometer method for detailed particle size analysis: General interpretation of hydrometer readings and test of method. Soil Sci 118(2):102–108. https://doi.org/10.1097/00010694-197408000-00007

Korte F, Spiteller M, Coulston F (2000) The cyanide leaching gold recovery process is a nonsustainable technology with unacceptable impacts on ecosystems and humans: the disaster in Romania. Ecotoxicol Environ Safe 46(4):241–245. https://doi.org/10.1006/eesa.2000.1938

Krumina L, Kenney JPL, Loring JS, Persson P (2016) Desorption mechanisms of phosphate from ferrihydrite and goethite surfaces. Chem Geol 427:54–64. https://doi.org/10.1016/j.chemgeo.2016.02.016

Kuyucak N, Akcil A (2013) Cyanide and removal options from effluents in gold mining and metallurgical processes. Miner Eng 50–51:13–29. https://doi.org/10.1016/j.mineng.2013.05.027

Ladeira ACQ, Ciminelli VST (2004) Adsorption and desorption of arsenic on an oxisol and its constituents. Water Res 38(8):2087–2094. https://doi.org/10.1016/10.1016/j.watres.2004.02.002

Liu HB, Chen TH, Frost RL, Chang DY, Qing CS, Xie QQ (2012) Effect of aging time and Al substitution on the morphology of aluminous goethite. J Colloid Interf Sci 385(1):81–86. https://doi.org/10.1016/j.jcis.2012.07.016

Madigan C, Leong YK, Ong BC (2009) Surface and rheological properties of as-received colloidal goethite (α-FeOOH) suspensions: pH and polyethylenimine effects. Int J Miner Proc 93(1):41–47. https://doi.org/10.1016/j.minpro.2009.05.005

Manar R, Bonnard M, Rast C, Veber AM, Vasseur P (2011) Ecotoxicity of cyanide complexes in industrially contaminated soils. J Hazard Mater 197:369–377. https://doi.org/10.1016/j.jhazmat.2011.09.095

Mansfeldt T, Höhener P (2016) Isotopic fingerprints of iron−cyanide complexes in the environment. Environ Sci Technol 50(14):7382–7388. https://doi.org/10.1021/acs.est.6b01565

Meeussen JCL, Keizer MG, De Haan FAM (1992) Chemical stability and decomposition rate of iron cyanide complexes in soil solutions. Environ Sci Technol 26(3):511–516. https://doi.org/10.1021/es00027a010

Mehra OP, Jackson ML (1958) Iron oxide removal from soils and clays by a dithionite–citrate system buffered with sodium bicarbonate. Clay Clay Miner 7:317–327. https://doi.org/10.1346/CCMN.1958.0070122

Moussavi G, Pourakbar M, Aghayani E, Mahdavianpour M (2018) Investigating the aerated VUV/PS process simultaneously generating hydroxyl and sulfate radicals for the oxidation of cyanide in aqueous solution and industrial wastewater. Chem Eng J 350:673–680. https://doi.org/10.1016/j.cej.2018.05.178

Prampolini G, Yu PY, Pizzanelli S, Cacelli I, Yang F, Zhao J, Wang JP (2014) Structure and dynamics of ferrocyanide and ferricyanide anions in water and heavy water: an insight by MD simulations and 2D IR spectroscopy. J Phys Chem B 118(51):14899–14912. https://doi.org/10.1021/jp511391b

Rader WS, Solujic L, Milosavljevic EB, Hendrix JL, Nelson JH (1993) Sunlight–induced photochemistry of aqueous solutions of hexacynoferrate(II) and (III) ions. Environ Sci Technol 27(9):1875–1879. https://doi.org/10.1021/es00046a016

Rennert T, Mansfeldt T (2001) Sorption of iron–cyanide complexes on goethite. Eur J Soil Sci 52(1):121–128. https://doi.org/10.1046/j.1365-2389.2001.00368

Rennert T, Mansfeldt T (2002a) Sorption of iron–cyanide complexes on goethite in the presence of sulfate and desorption with phosphate and chloride. J Environ Qual 31(3):745–751. https://doi.org/10.2134/jeq2002.0745

Rennert T, Mansfeldt T (2002b) Sorption and desorption of iron–cyanide complexes in deposited blast furnace sludge. Water Res 36(19):4877–4883. https://doi.org/10.1016/S0043-1354(02)00217-8

Rennert T, Kaufhold S, Mansfeldt T (2005) Sorption of iron–cyanide complexes on goethite investigated in long–term experiments. J Plant Nut Soil Sci 168(2):233–237. https://doi.org/10.1002/jpln.200421602

Rennert T, Kaufhold S, Mansfeldt T (2007) Identification of iron–cyanide complex in contaminated soils and wastes by Fourier transform infrared spectroscopy. Environ Sci Technol 41(15):5266–5270. https://doi.org/10.1021/es070492g

Roden EE, Zachara JM (1996) Microbial reduction of crystalline iron (III) oxides: influence of oxide surface area and potential for cell growth. Environ Sci Technol 30:1618–1628. https://doi.org/10.1021/es9506216

Shifrin NS, Beck BD, Gauthier TD, Chapnick SD, Goodman G (1996) Chemistry, toxicology, and human health risk of cyanide compounds in soils at former manufactured gas plant sites. Regul Toxicol Pharm 23(2):106–116. https://doi.org/10.1006/rtph.1996.0032

Sut-Lohmann M, Raab T (2017) Quick detection and quantification of iron–cyanide complexes using fourier transform infrared spectroscopy. Environ Pollut 227:64–72. https://doi.org/10.1016/j.envpol.2017.04.052

Sut-Lohmann M, Repmann F, Raab T (2014) Stability of Prussian Blue in soils of a former manufactured gas plant site. Soil Sedim Contam 23(5):504–522. https://doi.org/10.1080/15320383.2014.839626

Sut-Lohmann M, Repmann F, Raab T (2015) Retardation of iron-cyanide complexes in the soil of a former manufactured gas plant site. J Environ Sci Health Part A 50(3):282–291. https://doi.org/10.1080/10934529.2015.981116

Sweegers C, de Coninck HC, Meekes H, van Enckevort WJP, Hiralal IDK, Rijkeboer A (2001) Morphology, evolution and other characteristics of gibbsite crystals grown from pure and impure aqueous sodium aluminate solutions. J Cryst Growth 233(3):567–582. https://doi.org/10.1016/S0022-0248(01)01615-3

Szewczuk-Karpisz K, Krasucka P, Boguta P, Skic K, Sokolowska Z, Fijalkowska G, Wisniewska M (2018a) Anionic polyacrylamide efficiency in goethite removal from aqueous solutions: goethite suspension destabilization by PAM. Int J Environ Sci Technol 16(7):3145–3154. https://doi.org/10.1007/s13762-018-2064-5

Szewczuk-Karpisz K, Krasucka P, Boguta P, Skic K, Sokolowska Z, Fijalkowska G, Wisniewska M (2018b) Electrical double layer at

the gibbsite/anionic polyacrylamide/supporting electrolyte interface-adsorption, spectroscopy and electrokinetic studies. J Mol Liq 261:439–445. https://doi.org/10.1016/j.molliq.2018.04.030

Theis TL, Young TC, Huang M, Knutsen KC (1994) Leachate characteristics and composition of cyanide–bearing wastes from manufactured gas plants. Environ Sci Technol 28(1):99–106. https://doi.org/10.1021/es00050a014

Tiberg C, Sjöstedt C, Eriksson AK, Klysubun W, Gustafsson JP (2020) Phosphate competition with arsenate on poorly crystalline iron and aluminum (hydr) oxide mixtures. Chemosphere 255:126937. https://doi.org/10.1016/j.chemosphere.2020.126937

Violante A, Pigna M (2002) Competitive sorption of arsenate and phosphate on different clay minerals and soils. Soil Sci Soc Am J 66(6):1788–1796. https://doi.org/10.2136/sssaj2002.1788

Wei SY, Tan WF, Liu F, Zhao W, Weng LP (2014) Surface properties and phosphate adsorption of binary systems containing goethite and kaolinite. Geoderma 213:478–484. https://doi.org/10.1016/j.geoderma.2013.09.001

Wei YM, Du L, Deng X, Liu XY, Mei XX (2018) Alkaline–assisted leaching of iron–cyanide complex from contaminated soils. Chem Eng J 354:53–61. https://doi.org/10.1016/j.cej.2018.07.152

Wei YM, Wang F, Liu X, Fu PR, Yao RX, Ren TT, Shi DZ, Li YY (2020) Thermal remediation of cyanide–contaminated soils: process optimization and mechanistic study. Chemosphere 239:124707. https://doi.org/10.1016/j.chemosphere.2019.124707

Wisawapipat W, Kheoruenromne I, Suddhiprakarn A, Gilkes RJ (2009) Phosphate sorption and desorption by Thai upland soils. Geoderma 153(3–4):408–415. https://doi.org/10.1016/j.geoderma.2009.09.005

Wu CH, Lo SL, Lin CF (2000) Competitive adsorption of molybdate, chromate, sulfate, selenate, and selenite on γ-Al2O3. Colloid Surfaces A 166(1–3):251–259. https://doi.org/10.1016/S0927-7757(99)00404-5

Wu SY, Lian YW, Zheng H, Cai P, Pu YB (2012) Effect of preparation conditions on synthetic goethite. Environ Chem 31(10):1625–1630 (**(In Chinese)**)

Xiong J, Koopal LK, Weng LP, Wang MX, Tan WF (2015) Effect of soil fulvic and humic acid on binding of Pb to goethite–water interface: linear additivity and volume fractions of HS in the Stern layer. J Colloid Interf Sci 457:121–130. https://doi.org/10.1016/j.jcis.2015.07.001

Xiong J, Weng L, Koopal LK, Wang M, Shi Z, Zheng L, Tan W (2018) Effect of soil fulvic and humic acids on Pb binding to the goethite/solution interface: ligand charge distribution modeling and speciation distribution of Pb. Environ Sci Technol 52(3):1348–1356. https://doi.org/10.1021/acs.est.7b05412

Xu JL, Koopal LK, Wang MX, Xiong J, Hou JT, Lia Y, Tan WF (2019) Phosphate speciation on Al-substituted goethite: ATR–FTIR/2D–COS and CD–MUSIC modeling. Environ Sci: Nano 6(12):3625–3637. https://doi.org/10.1039/c9en00539k

Yan L, Xu Y, Yu H, Xin X, Wei Q, Du B (2010) Adsorption of phosphate from aqueous solution by hydroxy–aluminum, hydroxy–iron and hydroxy–iron–aluminum pillared bentonites. J Hazard Mater 179(1–3):244–250. https://doi.org/10.1016/j.jhazmat.2010.02.086

Zhang W, Liu WD, Lv Y, Li BJ, Ying WC (2010) Enhanced carbon adsorption treatment for removing cyanide from coking plant effluent. J Hazard Mater 184(1–3):135–140. https://doi.org/10.1016/j.jhazmat.2010.08.015

Zhang J, Liu L, Liang Y, Zhou JZ, Xu YF, Ruan XX, Lu YS, Xu ZP, Qian GR (2015) Enhanced precipitation of cyanide from electroplating wastewater via self–assembly of bimetal cyanide complex. Sep Purif Technol 150:179–185. https://doi.org/10.1016/j.seppur.2015.07.008